ATCZ175 InterOP PROJECT

Low-Cost WLAN Interference Emulator

Institute of Electrodynamics, Microwave and Circuit Engineering
Technische Universität Wien

Advisor:
Assoc. Prof. Dipl.-Ing. Dr.techn. Holger Arthaber

by
Christian Spindelberger BSc.

November 13, 2018

Contents

1 Introduction and Motivation

Goal of this work is to build a noise source with a digitally stepped output power level. This device is intended to be used as an interferer in the 2.4 GHz industrial, scientific and medical (ISM) band. It should emulate real traffic by generating noise bursts with modulated amplitudes and lengths. Special focus will lie on a strongly growing market, called Internet of Things (IoT). Aim of this branch is to provide communication for wireless devices like sensors or smart wearables. For instance, smart watches show received messages, incoming phone calls or record vitality data like the pulse rate.

In IoT, common standards like Bluetooth Low Energy (BLE) or Wireless LAN (WLAN) located in the 2.4 GHz and 5 GHz (no BLE) ISM band, are used for data transfer. Due to a increasing number of devices, traffic load grows and subsequently also more potential interferer exist. Although the functionality of WLAN and BLE provide techniques to prevent from such errors, performance is still limited.

In real life scenarios, many further kinds of standards like SigFox, ZigBee, HyperLAN, etc. are in the air. Thus, it becomes difficult to emulate all kind of these interferer with a software defined radio. Therefore, the noise source would be a much simpler approach for generating traffic. Real ISM band records serve data for a statistical model of channel occupation and amplitude distributions. With this knowledge, it is possible to modulate the required noise source.

2 Theory and Calculations

The introduced field of application for the noise source demands additive white gaussian noise (AWGN) on its output. Properties of such a signal are constant power spectral density over frequency $P(f) = \text{const.}$, normally distributed amplitudes in time domain and a autocorrelation function according to the delta distribution $r_{xx}(\tau) = \text{const.} \cdot \delta(\tau)$. Indeed such ideal conditions do not appear in reality and several noise types have to be taken into account for different frequency ranges. The main types and their advantages will be discussed in the following chapter about noise generators.

Of course the dynamic range, timing resolution and absolute output power must be determined for the design. With a radio frequency link budget, it will be shown which effects have to be considered for a correct analytical model.

2.1 Noise generators

Noise generators are typically used for noise figure (NF) measurements, which require a broadband AWGN output. To generate such a signal, several techniques exist.

The simplest one is based on utilizing thermal noise of a resistor and its power spectral density (PSD) may be altered by changing its temperature. According to equation 1 PSD can be easily calculated for a 50Ω resistor at a temperature T:

$$P_N = kT \quad [P_N] = \frac{\mathrm{W}}{\mathrm{Hz}} \tag{1}$$

At a first glance, this method impresses due to its simplicity, but it has several disadvantages. For a bandwidth of 20 MHz and room temperature T = 290 K, overall noise power equals −101 dBm, which is much lower compared to other techniques. Obviously, PSD can be increased by a higher temperature, but this is very impractical due to its linear behavior. If one would like to achieve 10 dB more power, temperature must become higher by a factor of 10.

Alternatively, shot noise current from diodes can be considered. The mechanism behind this technique can be described by random fluctuations which occur when electrons pass through a potential barrier, like in pn junctions. Diodes are usually biased in reverse direction. This causes a higher potential barrier and subsequently the power level rises. Figure 1 shows the typical biasing circuit of a noise diode in reverse direction. With the resistor R, the operating point of the noise diode can be adapted and capacitor C provides AC coupling to prevent from shorting the noise signal. With this method, power levels 30 dB higher than thermal noise at room temperature can be achieved. But a major disadvantage occurs due to device capacitance and carrier transport effects. The movement of electrons and holes in the depletion region is dominated by drift currents, but outside this area drift vanishes and much slower diffusion currents appear. Even if the depletion region is maximized through a higher biasing voltage, diffusion limits the PSD for high frequency application.

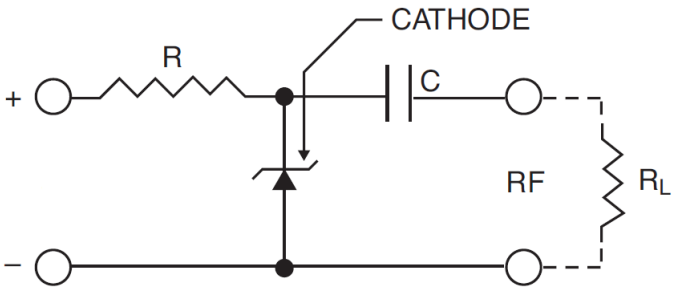

Figure 1: Typical diode biasing circuit

Current fluctuations in semiconductors like shot noise are described by a Poisson distribution ($p_P(n) \sim P(\lambda)$). The Poisson distribution expresses the probability of a number of events occurring in a fixed time if these events occur with a known average rate, and independently of the time since the last event. The parameter λ is equal to the expected number of electrons during a given time. It is remarkable, that for a high amount of electrons in the mentioned time interval, this function becomes indistinguishable from a Gaussian distribution ($p_G(x) \sim N(\mu, \sigma^2)$). This effect can be explained with the Central Limit Theorem (CLT). The CLT establishes that, in some situations, when independent random variables are added, their properly normalized sum tends toward a normal distribution, even if the original variables themselves are not normally distributed. In equation 3 we can see how the transformed normal probability density function (PDF) relates to the Poisson PDF.

$$p_P(n) = \frac{\lambda^n e^{-\lambda}}{n!} \sim P(\lambda) \tag{2}$$

$$p_G(x) = \lim_{\lambda->\infty} P(\lambda) = \frac{e^{-(x-\lambda)^2/(2\lambda)}}{\sqrt{2\pi\lambda}} \sim N(\lambda, \lambda) \tag{3}$$

Due to the high frequency limitations, state of the art noise sources use silicon avalanche diodes. They are more applicable because the avalanche effect does not suffer from device capacitance and carrier transport effects. Carriers in the depletion region gain energies in a high electrical field and then they collide with the crystal lattice. If the energy gained between collisions is large enough, then during collision another pair of carriers (electron and hole) can be generated. This is a random process and the intensity of avalanche noise is usually much larger than any other noise type. A further advantage is the frequency independent PSD, which is described with equation 4 (I(A)...Bias current, $\tau(s)$...Recombination time, B(Hz)...Bandwidth):

$$P_N(B) = \frac{2qI}{(2\pi B\tau)^2} \tag{4}$$

Due to the CLT, fluctuations in semiconductor junctions can be assumed Gaussian and independently distributed. Thus, two of three necessary conditions for AWGN are established (Gaussian, White). Only the PSD is not constant over the whole frequency range. Especially

for low frequencies, diodes suffer significantly from $\frac{1}{f}$ noise. Therefore, it has to be taken into account, that the $\frac{1}{f}$ corner frequencies do not collide with the used range. With this constraint, even the PSD can be assumed flat for a defined bandwidth, fulfilling all necessary conditions for an AWGN source.

2.2 Requirements

The noise source will be used in a WLAN test setup. During an user datagram protocol (UDP) transmission test between two WLAN cards the packet error rate (PER) is measured, while the noise source introduces interference.

The insertion loss seen by the source's output is approximately 16 dB. In the 802.11 standard it is mentioned that preambles of WLAN packets are detected down to −82 dBm and other kinds, like noise, with energy detection down to −62 dBm. Due to ISM band traffic records, we know that the peak envelope power is about −35 dBm. Thus, the required dynamic is DR = −35 dBm − (−82 dBm) ≈ 50 dB and the maximum output power equals P_{max} = −35 dBm + 16 dB ≈ −15 dBm. To compensate additional losses a power margin was introduced.

Reduced interframe spaces (RIFS) are specified in 802.11n standard and stand for the minimum allowed delay time between two WLAN packets. These dead times last for $2\mu s$ and also define the maximum required switching speed T_{sw} of the noise source.

P_{max}	−15dBm
DR	50dB
T_{sw}	2μs

Table 1: Requirements on the noise source

Let us have a look on the noise floor density which is −174 dBm/Hz. For a bandwidth of 20 MHz the total noise power equals −101 dBm. According to Table 1, this level must be boosted to −15 dBm, to reach the first design goal. The required gain of 86 dB cannot be reached by one single noise diode, several amplifiers have to be cascaded.

Due to their advantages described in chapter 2.1, an avalanche diode is utilized as first instance of the noise source. To describe the gain of a diode the excess noise ratio (ENR) is used in equation 5 for $T_0 = 290$K:

$$\mathrm{ENR} = 10 \cdot \log\Big(\frac{T_{0_E} - T_0}{T_0}\Big) \tag{5}$$

Typical noise diodes offer an ENR of 30 dB, so power amplifiers (PA) are needed to deliver the remaining gain of 56 dB. State of the art WLAN PAs perform a gain of about 30 dB. Thus, at least two PAs are necessary.

To be able to realize a dynamic switching of the available output power with a minimum resolution time of 2 µs, digitally stepped attenuators (ATT) can be used. Normally, such components offer a dynamic range of 32 dB. The required dynamic range of 50 dB can therefore be reached by two attenuators.

RF Link Budget

In RF link budgets the noise figure (NF) always plays an important role for system performance. As we are amplifying noise, one could think that the NF has an impact on output power due to the varying insertion loss of digitally stepped ATTs. To prove this hypothesis, an example has to be considered:

Let us assume a chain of one noise diode ($\mathrm{ENR} = 20\,\mathrm{dB}$), a PA ($\mathrm{G} = 30\,\mathrm{dB}$, $\mathrm{NF} = 6\,\mathrm{dB}$) and at the end an ATT with 32 dB insertion loss. According to formula 5, the equivalent noise temperature of the noise diode is $T_{0_E} = 29\,290\,\mathrm{K}$. With this reference temperature, the NF of PA and ATT can be recalculated with equation 6.

$$\mathrm{NF} = 1 + \frac{\mathrm{T_E}}{\mathrm{T_{0_E}}} \tag{6}$$

The recalculated NFs for PA and ATT are $\mathrm{NF_{amp}} = 0.13\,\mathrm{dB}$, $\mathrm{NF_{att}} = 12.22\,\mathrm{dB}$. According to Friis formula in equation 7, the overall NF of the given chain can be calculated.

$$\mathrm{NF_{tot}} = \mathrm{NF_1} + \cdots + \frac{\mathrm{NF_N} - 1}{G_1 \cdots G_{N-1}} \tag{7}$$

For the given parameters, we derive an overall NF of $\mathrm{NF_{tot}} = 0.2\,\mathrm{dB}$.

In conclusion, one sees that the high dynamic range has no impact on the overall output noise power. Therefore, NFs in the RF link budget can be neglected and formula 8 as an output power level estimate with respect to insertion losses of ATTs ($\mathrm{IL_{att}}$) and transmission lines ($\mathrm{IL_{tx}}$), may be used.

$$P_{out} = -174\,\mathrm{dBm/Hz} + \mathrm{BW} + \mathrm{ENR} + \mathrm{G_{amps}} - \mathrm{IL_{att}} - \mathrm{IL_{tx}} \tag{8}$$

3 Realization

According to the RF link budget from chapter 2.2, an amplifier chain with one noise diode, two PAs and ATTs has been created. Figure 2 shows the detailed grouping of the components. A bandpass filter is added to the chain, which offers some advantages discussed in the following.

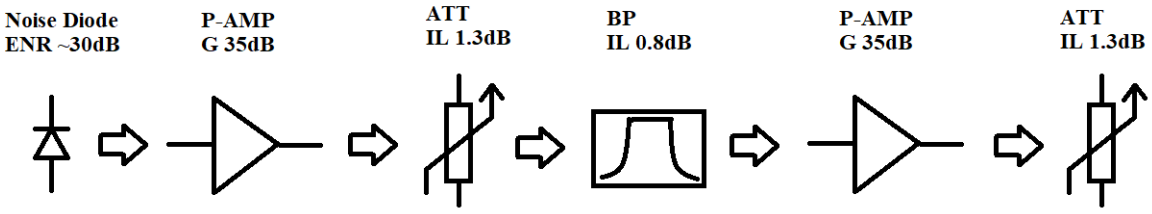

Figure 2: Noise source block diagram

PAs and ATTs are grouped in two stages. This has two main reasons. First, the ATTs are controlled by a parallel data bus with a microcontroller and have problems with cross talk if they are placed in a queue. So the bandpass filter and the following amplifier provide a higher isolation for proper functionality. But the filter has another advantage. The power spectra of noise diodes is broadband and also the PA has a bandwidth of more than 100 MHz. Thus, the bandpass filter ensures through spectral shaping, that the second amplifier is driven beyond its saturation region.

According to formula 8, the theoretically calculated output power for this chain is (BW = 20 MHz):

$$P_{out} = -174\,\mathrm{dBm/Hz} + 10 \cdot \log(20 \cdot 10^6\,\mathrm{Hz}) + 30\,\mathrm{dB} + 70\,\mathrm{dB} - 3.4\,\mathrm{dB} = -4.39\,\mathrm{dBm} \quad (9)$$

It must be mentioned, that no losses due to transmission lines or matching circuits are considered. Figure 3 shows the realized PCB board. It can be noticed, that small RF connectors are placed after each component for design verification. These parts are neither considered in calculation 9.

The noise source is modulated by an Arduino Nano microcontroller board with a ATMEGA328P chip and a maximum clock frequency of 16 MHz. Arduino provides a simple development chain, which makes it easy to program and flash the on-board logic. The microcontroller is placed on the upper right side and interfaces the used ATTs with an 8-bit parallel interface for each. But also faster controllers which are pin compatible, like from the Nucleo family with a clock speed of 80 MHz, can be utilized.

Details about the used components and layout guidelines are mentioned in chapters 3.1 and 3.2.

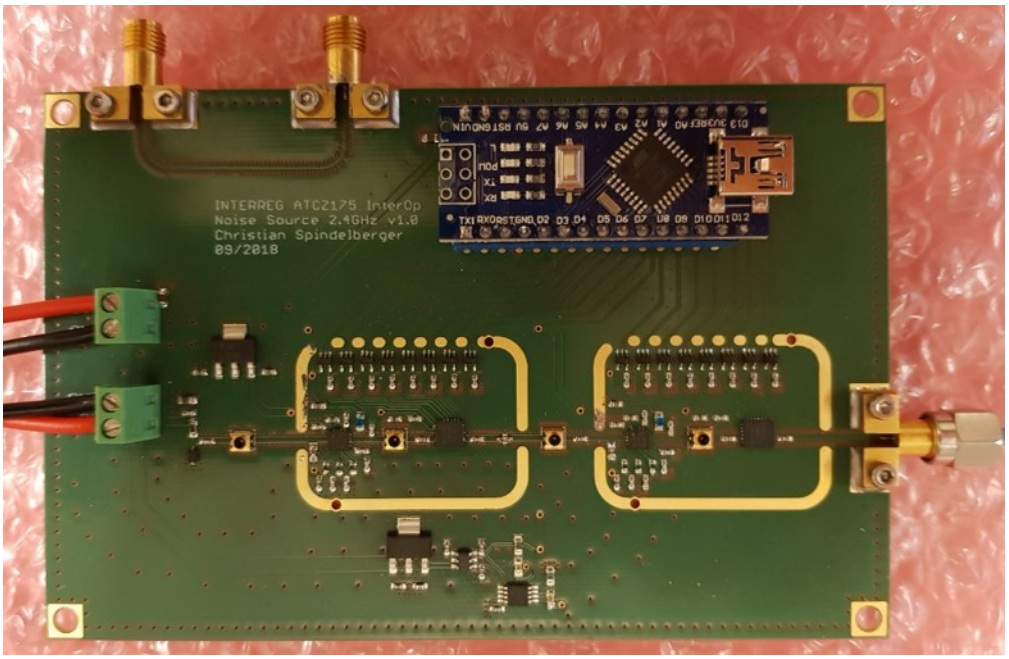

Figure 3: Picture of the noise source

3.1 Components and Schematics

In this chapter, properties of single components are discussed in general. Beside the noise source from figure 3, two further evaluation boards for the chosen PA and ATT have been developed. Please refer to the appendix, if a more detailed view on schematics and layouts is needed.

Noise Diode

The behavior of noise diodes strongly depend on their package and mounting. In this work the NS-301 diode from RF-Microwave is utilized, which has a SOT package and is applicable up to 3 GHz.

According to Figure 1, the diode is biased with an applied voltage in reverse direction. Depending on the voltage, PSD is influenced. For a high voltage, the spectrum gets flat, even for higher frequencies. But for lower voltages the ENR rises and flatness becomes worse. The specification sheet states that the optimum use case is an ENR of 30 dB at a reverse current of 8 mA, but no dimension recommendations. Therefore, the correct series resistor and voltage must be determined empirically to achieve this operating point.

The AC coupling capacitor prevents the diode from being shorted by the following circuit elements. If the noise source is used for broadband applications, the insertion loss characteristic can have a major impact on performance due to resonance effects.

Power Amplifier

Manufacturers like Microchip provide a huge variety of different PAs for WLAN applications. In this project, the SST12LP15A (figure 4) is used with a gain of 35 dB and a linear output

power of 29 dBm, which satisfies requirements from Table 1. Furthermore, external biasing through a reference voltage of 2.9 V is necessary. Please have a look on the overall schematic to see the detailed solution.

In figure 4 we can see the input matching coil L = 2.2 nH and output matching capacitor C = 2.7 pF. Due to uncertainties about material parameters (ϵ_r) and component properties the input- and output matching elements may change. Therefore, the evaluation board is used to characterize the PA on its own and verify proper matching conditions.

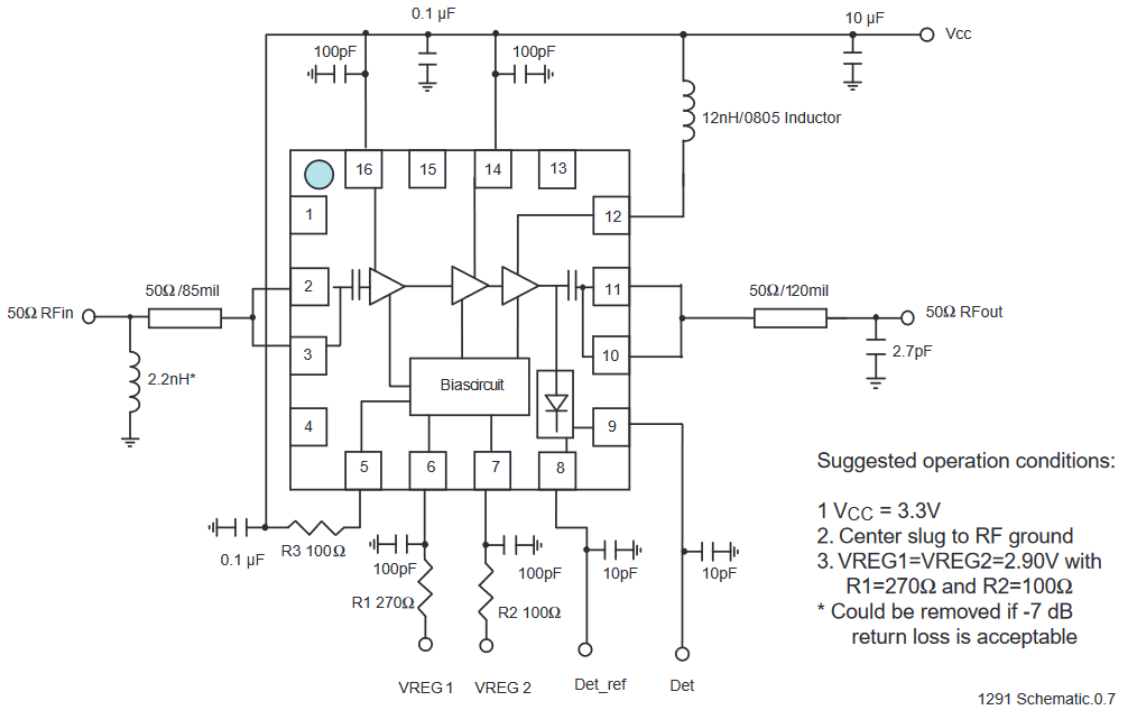

Figure 4: Schematic power amplifier

Attenuator

Digitally stepped ATTs have a dynamic range of typically 30 dB and a fast switching speed (settling time ≈ 100 ns). Unfortunately, some ATTs do not have a defined output state during switching. Hence, the required dynamic for this application is not feasible. Thus, a glitch-free 7bit ATT (F1950) from IDT is used, which yields a maximum settling time of 400 ns.

Figure 5 shows the exact realization with a parallel interface, connected with logic level converters. Here, the decoupling capacitors at the power supply pins of the converters must be emphasized. Especially, for a 2-layer design where no layer separation for digital and analog paths can be realized, prudent decoupling is necessary.

Design recommendations make use of high AC coupling capacitors of 1 nF. This seems not to be necessary for WLAN applications. A design with $C = (2\pi 50 \cdot 1.5 \cdot 10^9)^{-1} = 2\,\text{pF}$ for a cutoff frequency of 1.5 GHz would be a better choice for reducing insertion loss and saturation effects.

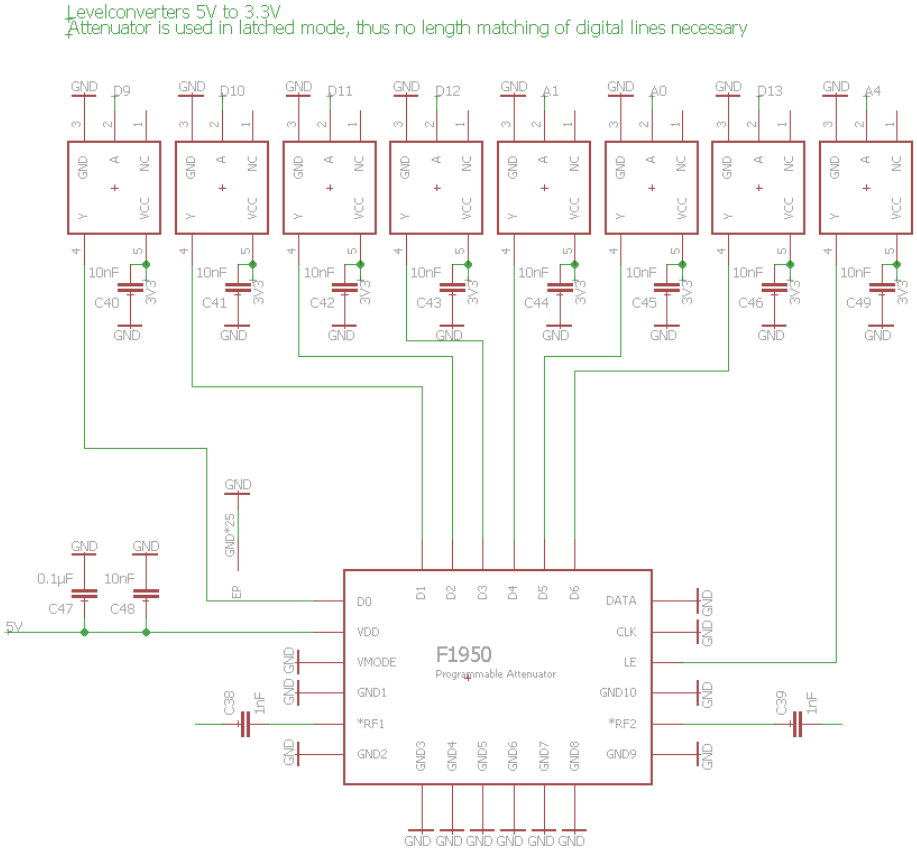

Figure 5: Schematic attenuator

3.2 Layout

The noise source is used in WLAN channel 1, centered at 2.412 GHz with a bandwidth of 20 MHz. As this is small band, dispersion issues for transmission line design can be neglected. This allows us to use a standard *FR4* substrate material with an $\epsilon_r = 4.6$ and a thickness of 1 mm. Unfortunately, the dielectric constant is defined as a mean value for a fixed frequency of 10 MHz. Thus, changes of ϵ_r over frequency must be considered.

The package of the utilized PA and ATT have a pitch of 0.5 mm and the microstrip line width for the given substrate thickness is about 2 mm wide. Hence, microstrip lines can only be used in combination with tapered structures, which is suboptimal. Consequently, co-planar ground topology is used, which offers several advantages for a proper design. In Figure 6, one can find the cross sectional area of the used waveguide.

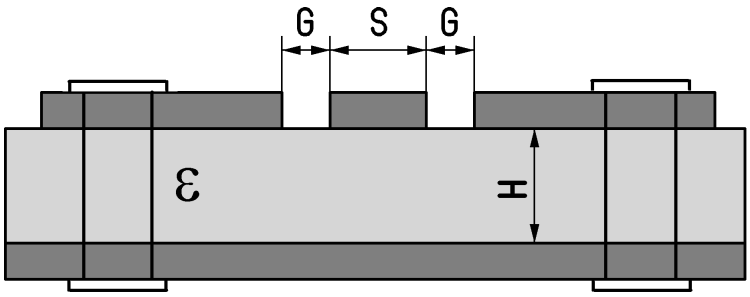

Figure 6: Co-planar ground wave guide

Due to the slot width G and transmission line width S, two parameters can be changed to maintain a more narrow width S, which fits the given pitch. Furthermore, co-planar ground wave guides are relatively insensitive on ϵ_r changes. As a compromise of the used components, the transmission line parameters for $Z_0 = 50\Omega$ impedance can be found in Table 2.

G	0.15mm
S	0.7mm
H	1mm

Table 2: Transmission line parameters

Manufacturing tolerances may have a crucial impact on the design goals. The width G of the gap should be in a region where process deviations are in a small scale. Otherwise, transmission line parameters will change. Furthermore, vias should be placed as close as possible to the ground plane and the distance between them should not exceed $\frac{\lambda}{10}$ to create almost ideal conditions.

In Figure 7, the layout of one amplifier-attenuator cascade is depicted. On the upper part, eight level converters are placed in parallel. In order to avoid additional ripple effects on the power supply due to switching the attenuators, bypassing capacitors with proper vias are needed. Therefore, a short example about calculating the right via size is mentioned below.

Parasitic capacitance and inductance may degrade circuit performance seriously, especially for bypassing capacitors. In the following equation for calculating via inductance, all dimensions are in mm. Obviously, reactance is frequency dependent. This effect is introduced by the transition time T_{10-90} of digital signals.

$$\mathrm{L} = 0.2 \cdot h \cdot \left[ln\left(\frac{4h}{d}\right) + 1 \right] \quad [\mathrm{L}] = \mathrm{nH} \tag{10}$$

Example: via length h = 1.55mm, via diameter d = 0.2mm, $T_{10-90} = 1\mathrm{ns}$

$$\mathrm{L} = 1.375\mathrm{nH} \quad X_L = \frac{\pi L}{T_{10-90}} = 4.32\Omega \tag{11}$$

A value of $4.32\,\Omega$ may not be sufficiently low to shunt off high frequency currents from a chip. This problem can be counteracted with placing several vias in parallel. Another approach is to use several bypassing capacitors in parallel. The effective radius, within this effect works, is equal to $\frac{l}{12}$, where l is the electrical length of a rising edge.

In this design, vias with a diameter of $0.4\,\text{mm}$, which have an inductance of $0.66\,\text{nH}$ at a layer thickness of $1\,\text{mm}$, are used. To ensure a low parasitic ground connection, several vias at the bypassing capacitors have been placed in parallel.

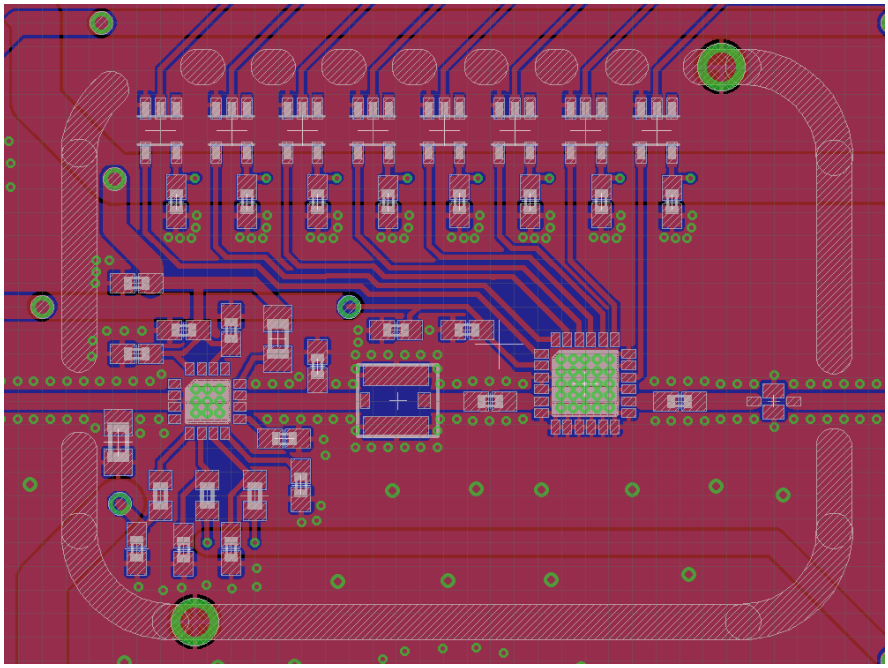

Figure 7: Layout of the amplifier attenuator cascade

Furthermore, the cascade depicted in Figure 7, has an additional surrounding shielding. The thick grey line, which is interrupted at several points shows the cut out of the solder resist. This shielding can be assembled in order to restrain additional crosstalk between the second cascade.

Of course, a more compact design would be possible, but PCB assembly was done by hand and this affords more space between components.

4 Measurements

This chapter is about all necessary measurements for characterizing the built noise source in Figure 3. Only the transmission line characteristics and PA matching was measured on the according evaluation boards.

4.1 Transmission Line

As discussed in chapter 3, the boards are all finished on *FR4* prototype material. A major issue that appears for prototype manufacturing is the inadequate definition of the dielectric constant ϵ_r over frequency. For this material an $\epsilon_r = 4.6$ at 10 MHz is given. For design verification, a 50Ω co-planar strip line has been realized.

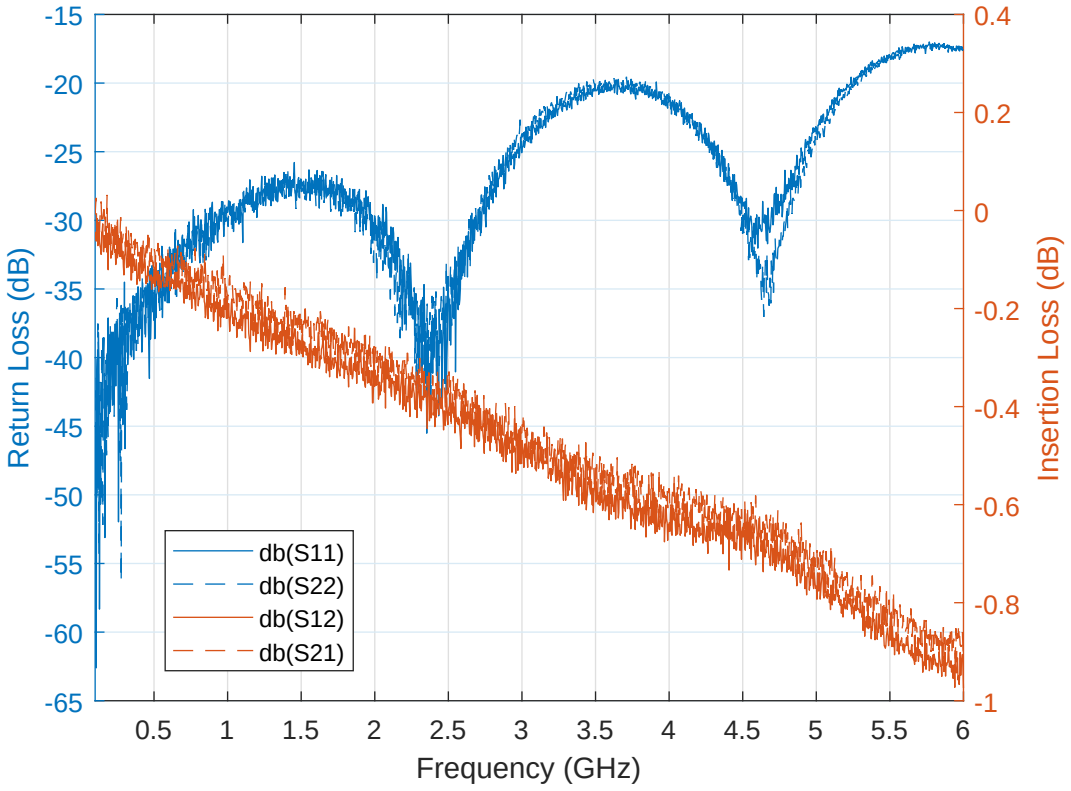

Figure 8: Transmission Line S-Parameters

Figure 8 shows the S-Parameters of the transmission line on the ATT evaluation board. This trace is 34.98mm long and has an attenuation of −0.381dB. But reflections possibly do not arise from the transmission line only. Due to the connectors, resonance effects in the return loss parameters S_{11} and S_{22} visualize. In addition to this, the data sheet of the used connector (Rosenberger 32K243) provides formulas for insertion loss IL and voltage standing wave ratio VSWR:

$$\mathrm{IL} \leq 0.03\sqrt{2.4\,\mathrm{GHz}}(\mathrm{dB}) = 0.047\mathrm{dB} \tag{12}$$

$$\mathrm{VSWR} \leq 1.1 + 0.02 \cdot 2.4\,\mathrm{GHz} = 1.14 \tag{13}$$

So the recalculated insertion loss is $-0.287\,\mathrm{dB}$ which stays almost the same. Furthermore, a VSWR of 1.14 corresponds to a return loss of $-23.69\,\mathrm{dB}$. The measured return losses S_{11} and S_{22} at 2.4 GHz are both not in the range of the connector specifications 12 and 13. Therefore, the transmission line can be assumed to have an impedance of $50\,\Omega$.

4.2 Diode Biasing

In Chapter 2, it has been mentioned that the right biasing conditions must be determined empirically. Normally, manufacturers provide detailed specifications of their testing conditions. For the used diode NS-301 from RF Microwave this is not the case. There is no information about maximum ratings, only achievable ENR and reverse current.

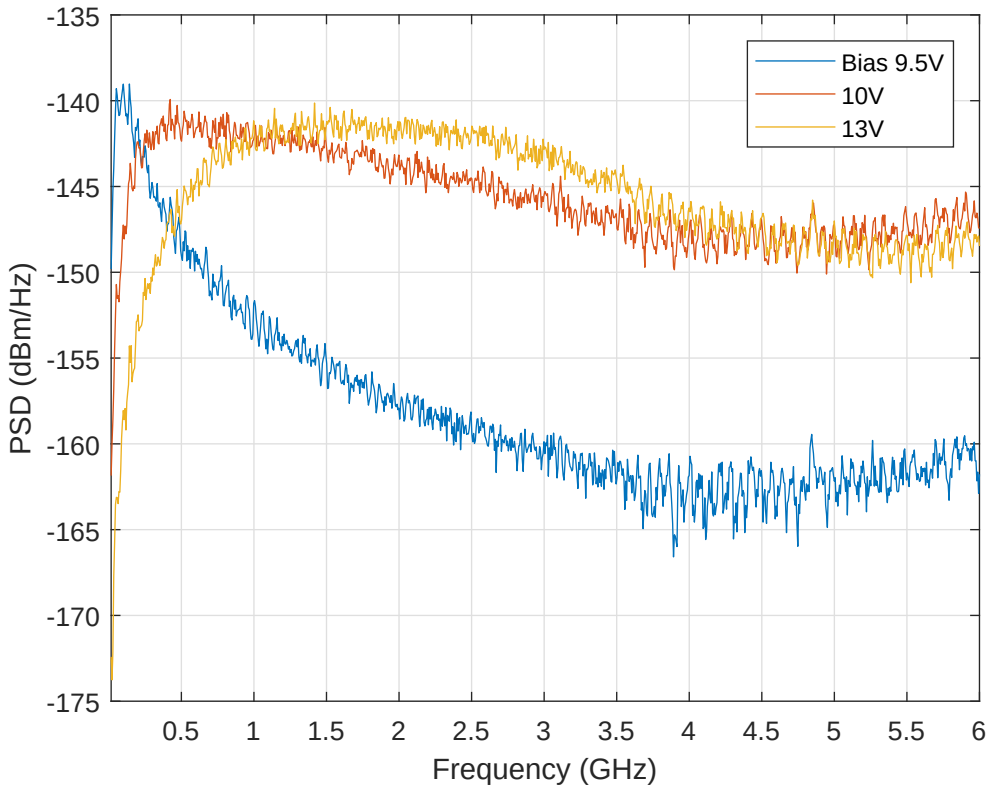

Figure 9: PSD of the used diode for different biasing voltages

According to the manufacturer, for 8 mA reverse bias current an ENR of approximately 30 dB should be possible up to 3 GHz. An application note about a similar diode gives an idea in

which scale biasing conditions should be adapted. Therefore, a 875 Ω series resistor and a maximum biasing voltage of 13 V according to Figure 1, has been adapted.

Figure 9 depicts the PSD for different biasing voltages. The avalanche effect starts at approximately 9.5 V and has its maximum below 500 MHz with a strong decay for higher frequencies. For 10 V and 13 V biasing conditions, one can notice that for higher voltages the PSD becomes more flat. An optimum biasing setting has to be found, because the higher the reverse voltage gets, the maximum ENR decreases.

For 2.412 GHz, it turned out a biasing voltage of 13 V offers maximum ENR of 32 dB.

4.3 Power Amplifier Matching

Microchip recommends the matching of the PA according to Figure 4. The input matching circuit consist of a 2.2 nH coil and a 85 mil long transmission line. Unfortunately, the measurement results of the PA evaluation board were not sufficient. The return loss S_{11} was above −7 dB. Hence, a smaller coil with 1.8 nH was used and led to a return loss of −12 dB at 2.4 GHz (Figure 10).

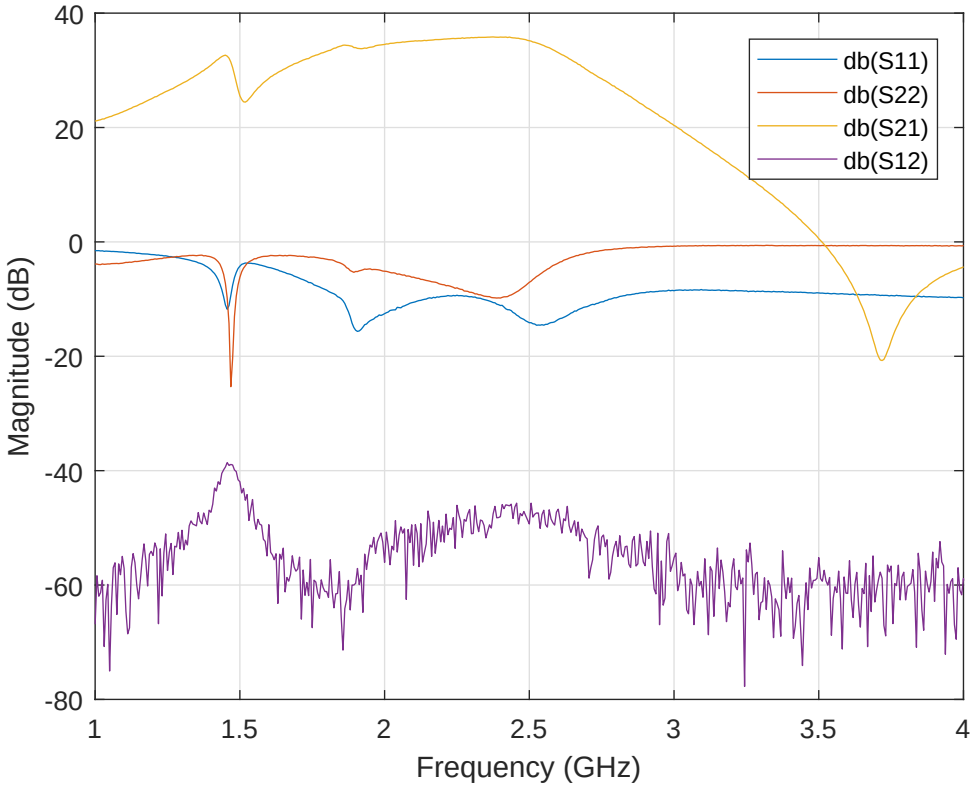

Figure 10: Power amplifier input matching

Microchip does not provide information about stability which is crucial for high gain applications. Rollet's factor gives information about unconditional stability.

$$\mathrm{K} = \frac{1 - |S_{11}|^2 - |S_{22}|^2 + \Delta^2}{2|S_{12}S_{21}|} \quad \Delta = S_{11}S_{22} - S_{21}S_{12} \tag{14}$$

So for a center frequency of 2.412 GHz and 20 MHz bandwidth, the K-factor is always bigger than 1, which states that the device is unconditionally stable. This calculation was also confirmed by the commissioning of the whole noise source from Figure 3.

4.4 Absolute Output Power

The overall output power was measured with an average power meter with a bandwidth from 10 MHz to 6 GHz. With this absolute power, the PSD of the spectrum analyzer which can be found below in Figure 11 was calibrated. Absolute power ratings can be found in Table 3.

BW (MHz)	Power (dBm)
5990	11.68
20 @ 2.412 GHz	-2.67

Table 3: Output power of the noise source

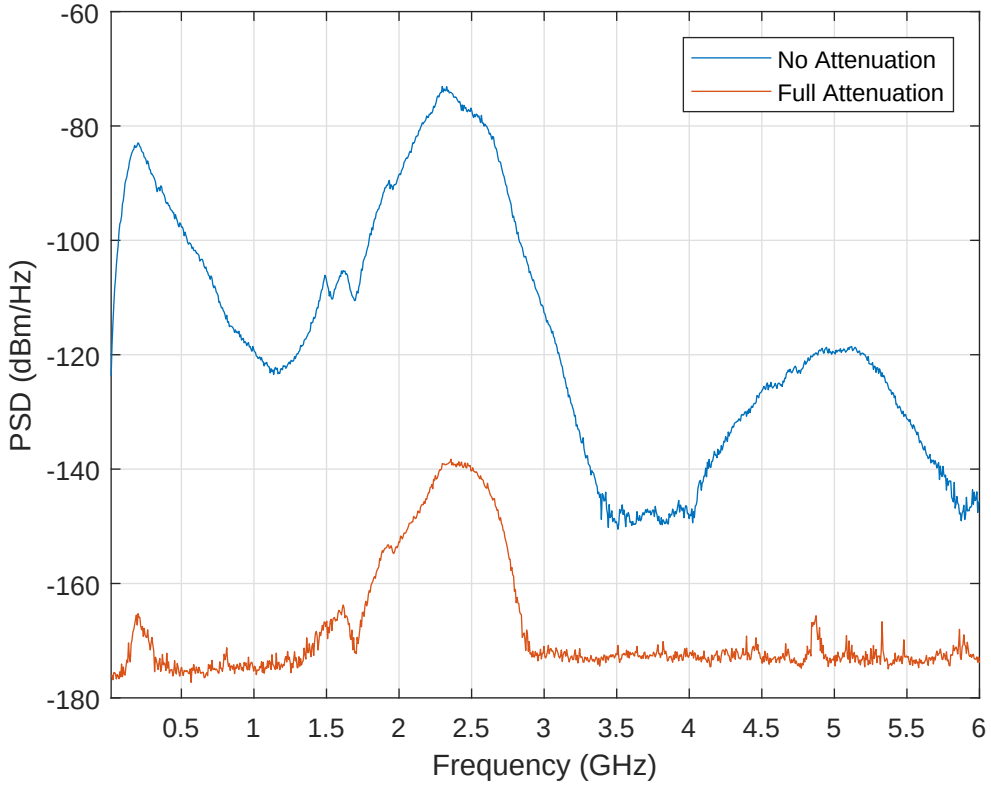

Figure 11: Noise source PSD

An output power of -2.67 dBm at 20 MHz bandwidth requires an overall gain of 97.33 dB.

From equation 9 an output power of −4.39 dBm, which is more than 2 dB lower, was expected. This can be explained through the higher ENR which is 32 dB instead of 30 dB.

4.5 Dynamic Behavior

The IDT F1950 ATT promises a glitch free transition between states with a maximums settling time of 400 ns. In Figure 12 the output envelope of the first ATT after the noise diode is depicted. For this measurement, a maximum switching speed of the Arduino Nano (discussed in chapter 3), which is 610.5 kHz was realized. For sure, faster switching speed is possible with pin compatible Nucleo boards, which have a 80 MHz clock frequency, but for measuring settling time, this is no issue.

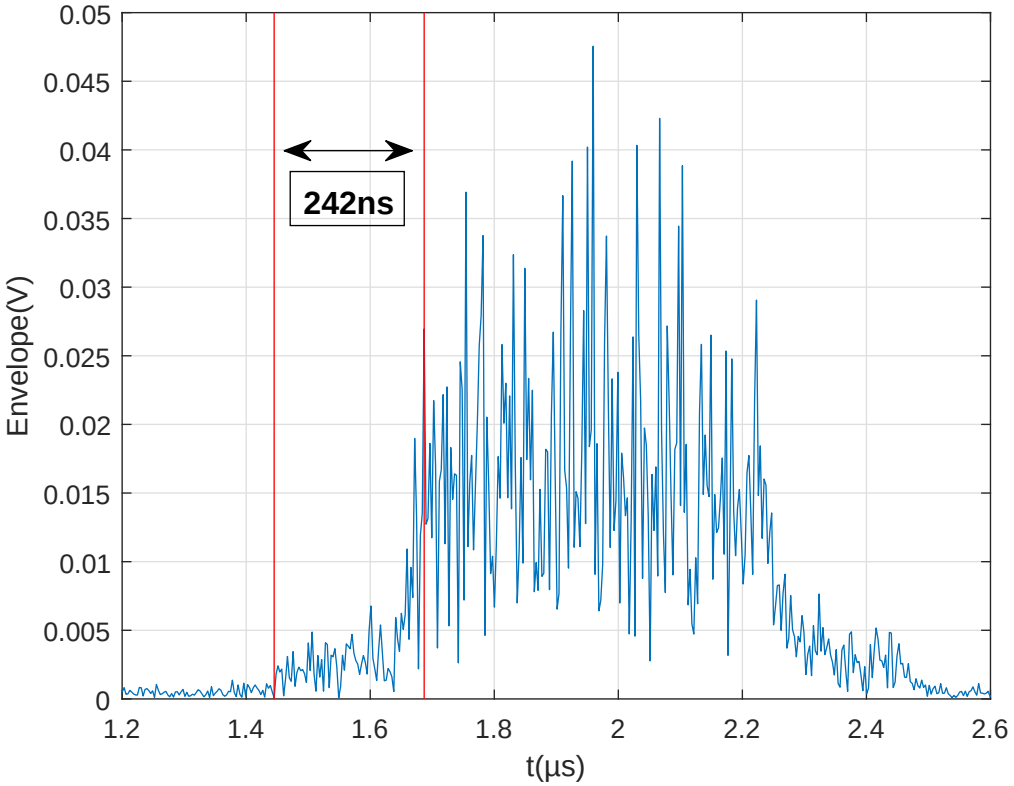

Figure 12: Switching delay of the first attenuator

Figure 12 shows transition between maximum and minimum attenuation (31.75 dB and 1.3 dB). Red lines mark the settling region, which is 242 ns long. Thus, the required timing resolution of 2 µs (Table 1) is feasible.

5 Conclusion

The goal of the project was to implement a noise source with a digitally stepped output power level. Desired dynamic range was 50 dB, a maximum power of −15 dBm and switching times up to 2 µs. Indeed, the realized circuit achieves a dynamic of 63.5 dB, output power of −2.67 dBm with 20 MHz bandwidth and a timing resolution of up to 484 ns. In summary it can be said, therefore, that all design goals have been reached successfully.

Although WLAN traffic is also present in the 5 GHz ISM band, this source is restricted to 2.4 GHz region for a first approach. Certainly, it is possible to use this concept for higher frequency applications. Noise diodes are available up to frequencies of 18 GHz with a compareable ENR as well as power amplifiers and attenuators.

Obviously this type of source is broadband, if adjacent channel interference should be emulated like it happens for instance between WLAN and BLE advertiser channels, another design concept must be considered. A promising technique would be to amplify narrow band noise and mix it up to the desired center frequency. But several problems have to be taken into account. Due to the local oscillator properties, variations in the CCDF may arise and AWGN assumption must be discarded.

On the one hand, it was shown how simple it is to implement a digitally controlled noise source for 2.4 GHz ISM band applications. If it is necessary higher frequencies can be reached with available products. On the other hand, if more degrees of freedom are required for adjacent channel interference a more complicated scheme is needful.

A Firmware & Matlab User Guide

On the InterOp homepage[1] different firmware versions and a Matlab class has been provided for an appropriate use of the presented noise source. Basically, two firmwares exist. The first one is utilized for the time-quantized modulation technique and the second one implements the modulation of on-/off-times as well. In order to understand these modulation techniques, please refer to the measurement campaign report[2]. For the whole example codes the sources noise diode has been powered with 13 V (current limit 100 mA) and the remaining components with 4.2 V (current limit 500 mA).

A.1 Firmware Considerations

The communication between the noise source and Matlab is realized by a serial interface over USB. It is necessary to desolder the diode between USB power supply and the chip on the Arduino Nano board. Otherwise it is not possible to establish a serial data exchange while the external power supply is running. In the following possible configurations and settings are discussed.

Time-Quantized Emulation

First of all, it is necessary to flash the correct firmware to the microcontroller. In the Arduino IDE one can read and modify the respective code. The two most important parameters which can be changed in the code only are `set_delay` and `array_length`. `set_delay` defines the time quantization length in microseconds and is set per default to 1 ms. The `array_length` variable declares the array length of the power levels generated in Matlab. Be careful with this parameter, too large values may cause an unstable behavior of the controller (default array length is set to 500).

Modulated Noise

If it is required to modulate on- and off-times as well, the second firmware must be utilized. In this case only the `array_length` has to be modified. Per default, this value is set to an array length of 200. Because of the additional arrays corresponding to on- and off-times, the memory space allows less samples compared to time quantization method. Again the on- and off-times are in microseconds.

A.2 Matlab Implementation

A Matlab class for interfacing the noise source is available to download. In the compressed file one can find also an example file `main` which introduces all available commands.

`obj.start_emulation()`: Starts the emulation sequence corresponding to the stored values of the power levels, on-, and off times.

`obj.stop_emulation()`: Stops the emulation sequence and sets maximum attenuation.

[1] `http://www.interreg-interop.eu/results/wlan_interference_analysis/low_cost_interference_emulator/`

[2] `http://www.interreg-interop.eu/results/wlan_interference_analysis/measurement_campaign/`

`obj.delete()`: Deletes the created communication instance.

`obj.stream_custom_data(emulation_mode, att_vals, 'On_times', on_times, 'Off_times', off_times)`: Makes it possible to stream custom values to the noise source.

`emulation_mode`: time quantized noise, modulated noise.

`att_vals`: row vector, attenuation values are quantized with a resolution of 0.25 dB between 0 dB and 63.5 dB.

`on_times`: row vector, positive on-time values (μs).

`off_times`: row vector, positive off-time values (μs).

`obj.stream_sequence(emulation_mode, array_length, pdf_power, 'PDF_on', pdf_on, 'PDF_off', pdf_off, 'bandwidth', BW)`: With this function, one can use created random variables to stream an emulation sequence to the noise source.

`emulation_mode`: time quantized noise, modulated noise.

`array_length`: positive scalar, defines the maximum amount of values gained from one random variable.

`pdf_power`: random variable, power level PDF, e.g., Laplace or Kernel. (dBm)

`pdf_on`: random variable, on-times PDF, e.g., Laplace or Kernel (μs).

`pdf_off`: random variable, off-times PDF, e.g., Laplace or Kernel (μs).

`BW`: positive scalar (Hz), describes the equivalent bandwidth of noise as reference power level relative to the power levels gained from the statistics. ($N_p = -174\,\mathrm{dBm/Hz} + 10\log_{10}(\mathrm{BW})$) With this reference power level the attenuation values are calculated with a resolution of 0.25 dB between 0 dB and 63.5 dB.

B Component List

Bezeichnung	ID	Hersteller
Power Amplifier	SST12LP15A	Microchip
Attenuator	F1950	IDT
Attenuator	HMC1119	Analog
Bandpass	DEA162450BT-1295A1	TDK
Level Converter	SN74LV1T34	TI
SMA	32K243-40ML5	Rosenberger
Test Connector	MS-156HF	Hirose
Shielding	Masach Serie 32.3x23.8x9mm	Masach Technologies
Power Connector	Wire-to-board	RS
LDO-5V	LM2937	TI
Reference Voltage	MAX6070	Maxim Integrated
Dual Opamp	OPA2192	TI
R 4.02k 0.1%	PHP00603E4021BST1	Vishay
R 25k 0.05%	PLT0603Z2502AST5	Vishay
L 12nH	LQW18AN12NG0ZD	Murata
L 2.2nH	LQW18AN2N2D0ZD	Murata
C 0.1µF	CGA2B3X7R1E104M050BB	TDK
C 100pF	GRM1555C1H101FA01J	Murata
C 10nF	VJ0402Y103JXJPW1BC	Vishay
C 10pF	GCQ1555C1H100FB01D	Murata
C 10µF	ZRB15XR61A106ME01D	Murata
C 2.7pF	GCQ1555C1H2R7WB01D	Murata
C 10µF	ZRB18AR61E106ME01L	Murata
C 1nF	VJ0402Y102JXXCW1BC	Vishay
C 3pF	GCQ1555C1H3R0WB01D	Murata
R 100	ERJ-PA2D1000X	Panasonic
R 270	ERJ-PA2D2700X	Panasonic
R 875	ERJ-P03F8660V	Panasonic
R 500	ERJ-P03F4990V	Panasonic

C Schematic and Layout

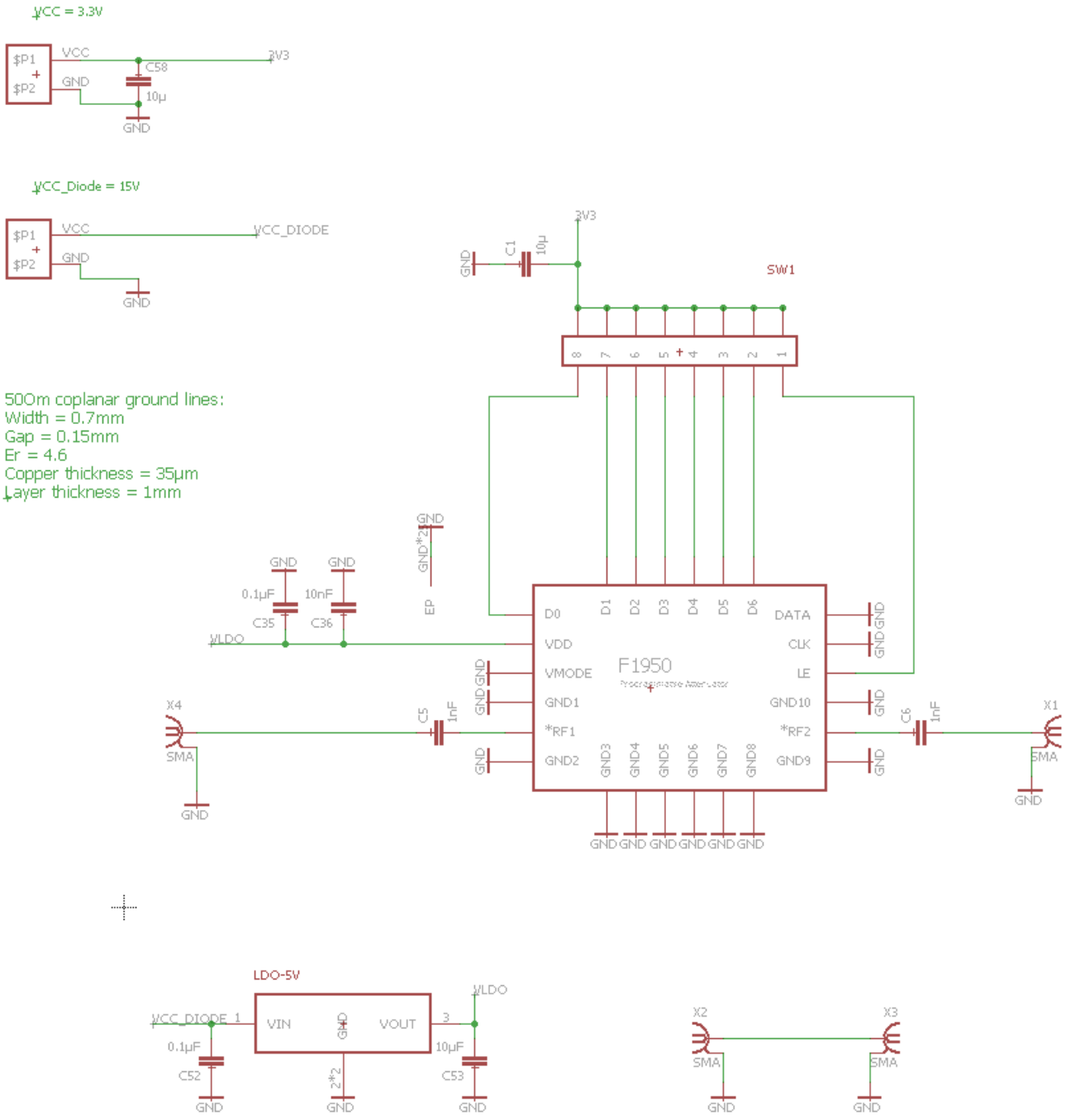

Figure 13: Attenuator Schematic

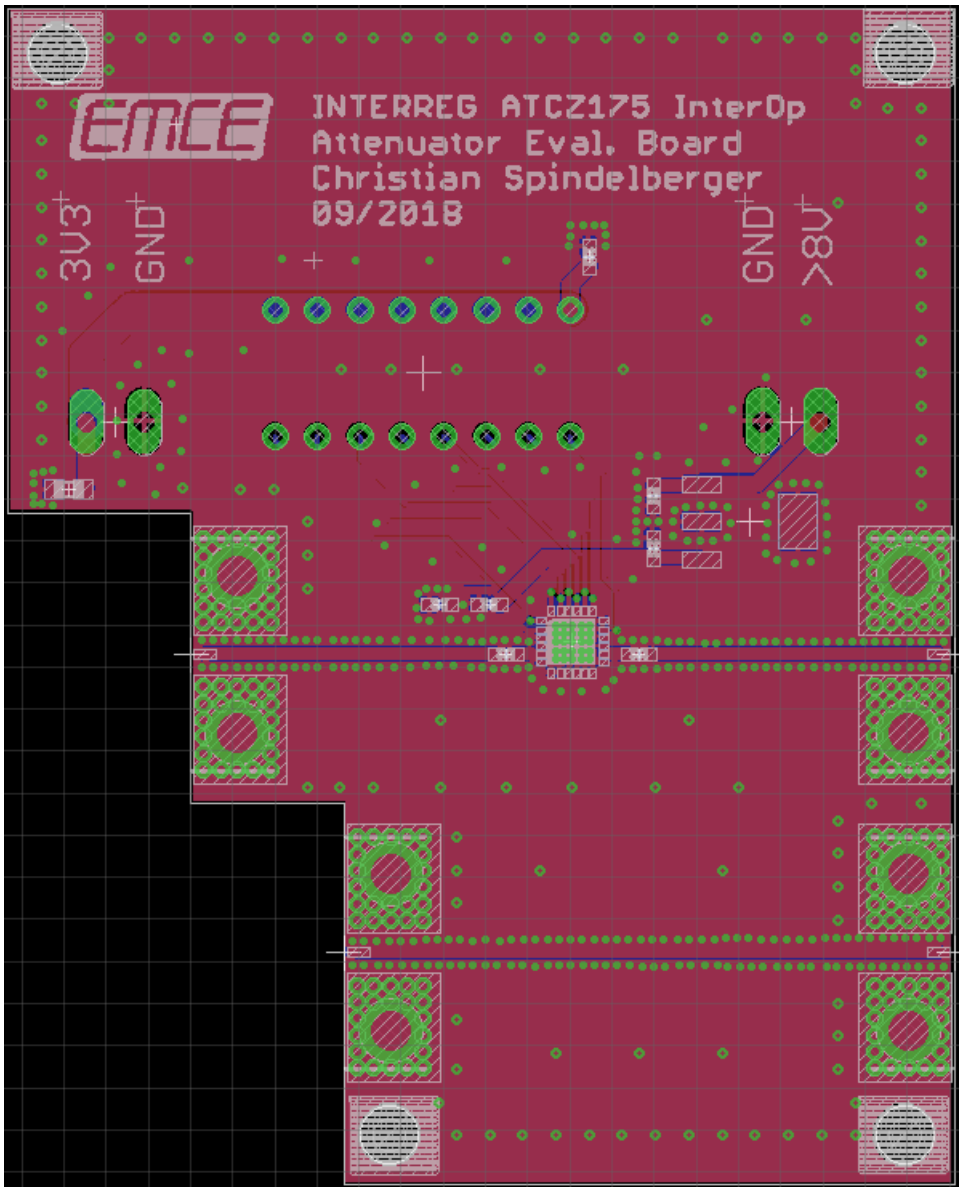

Figure 14: Attenuator Layout

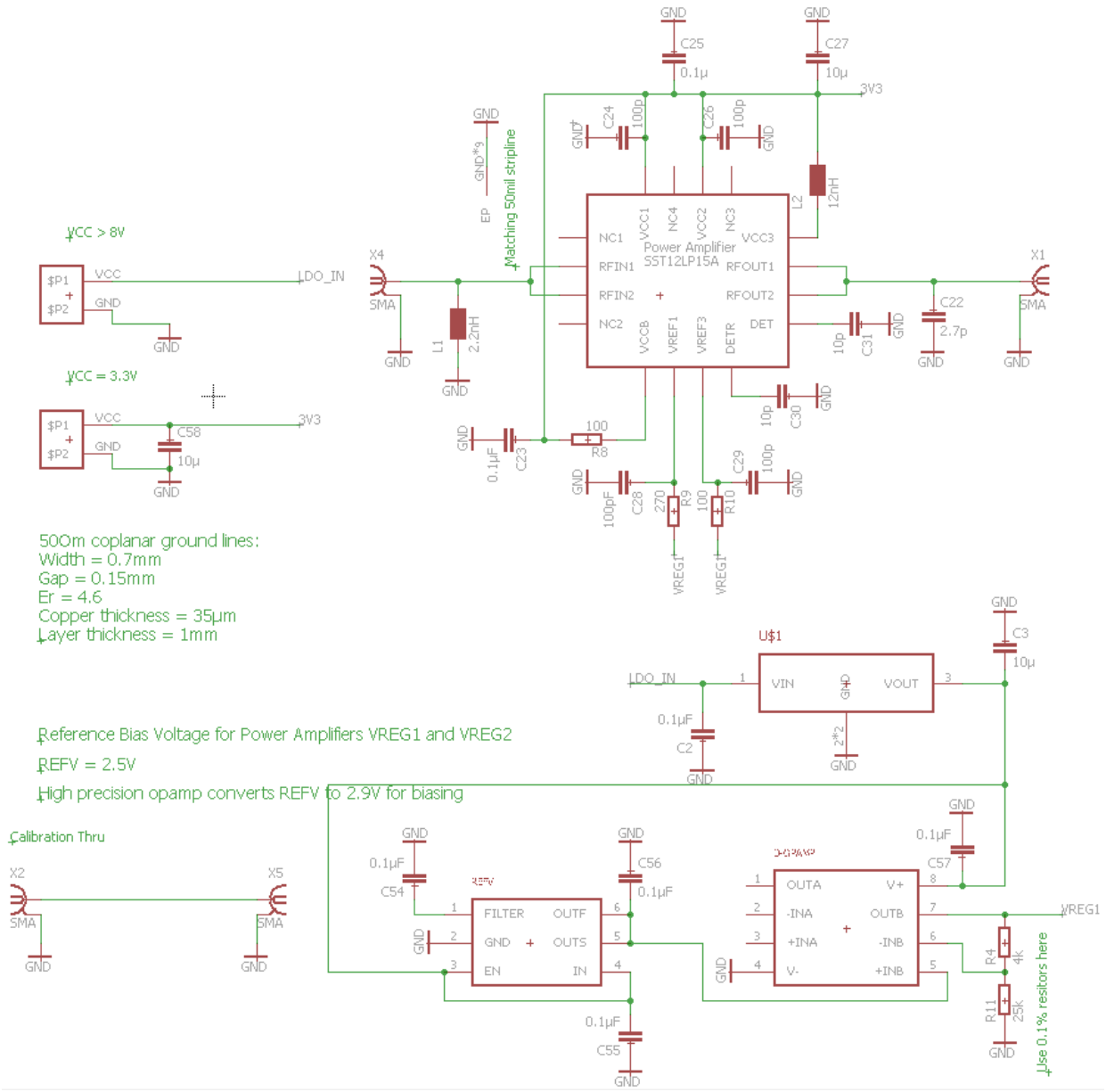

Figure 15: Power Amplifier Schematic

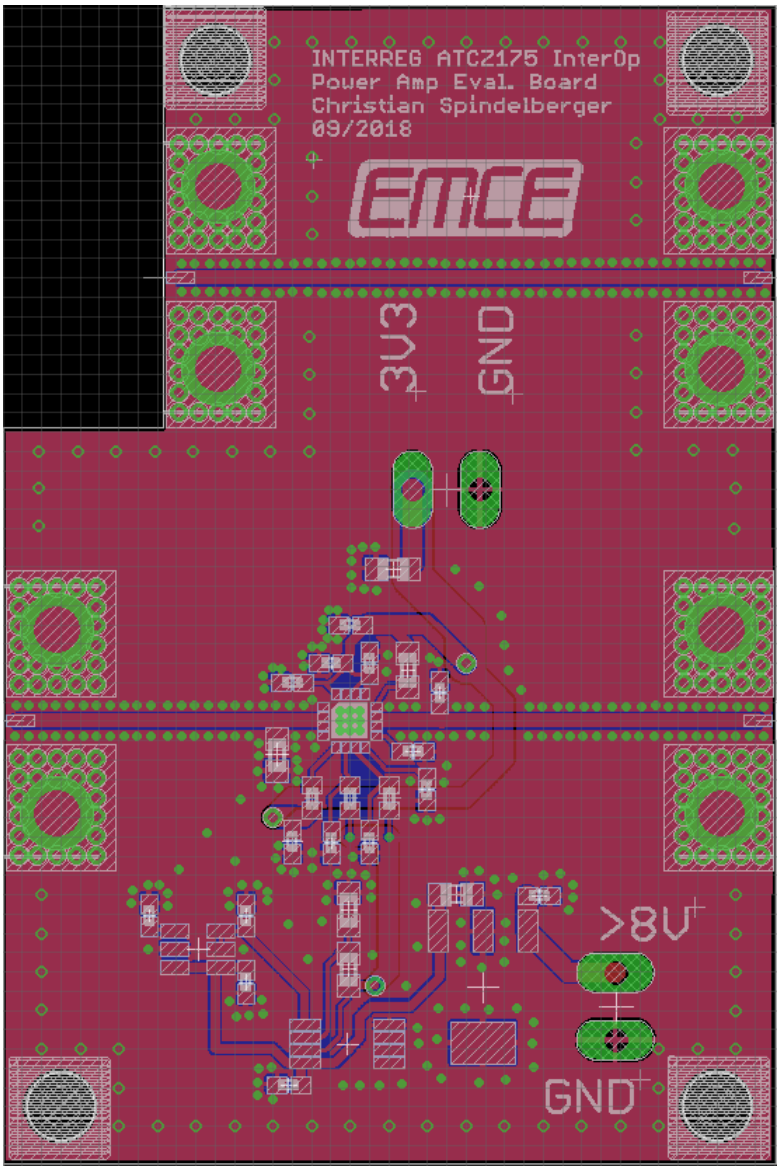

Figure 16: Power Amplifier Layout